JOURNAL OF SOLID STATE CHEMISTRY 93, 183–192 (1991)

Coordination and Valence of Niobium in TiO_2–NbO_2 Solid Solutions through X-Ray Absorption Spectroscopy

MARK R. ANTONIO,*† INHO SONG, AND HISAO YAMADA†

†*BP Research, Research Center Warrensville, 4440 Warrensville Center Road, Cleveland, Ohio 44128; and Department of Materials Science and Engineering, Case Western Reserve University, Cleveland, Ohio 44105*

Received April 2, 1990; in revised form January 18, 1991

The coordination and valence of niobium in TiO_2–NbO_2 solid solutions, $Nb_xTi_{1-x}O_2$ (for $0.1 \leq x \leq 1.0$), were studied by Nb K-edge X-ray absorption spectroscopy (XAS) as a function of Nb composition, x. Ten single-phase compositions in the $Nb_xTi_{1-x}O_2$ solid solution with the rutile structure were examined: $x = 0.1, 0.2, 0.32, 0.4, 0.5, 0.6, 0.7, 0.8, 0.9$, and 1.0. Analysis of X-ray absorption near edge structure (XANES) data shows that the position of the preedge absorption shifts to higher energy with decreasing Nb concentration, indicating that the ratio of Nb^{5+} to Nb^{4+} is larger at low Nb concentrations than at high ones. The extended X-ray absorption fine structure (EXAFS) analysis indicates that the average Nb–O interatomic distance increases nearly linearly with increasing Nb concentration. This structural modification of the oxygen environment about niobium suggests that an increasing fraction of Nb ions (i.e., Nb^{5+}) occupy tetrahedral interstitial sites with decreasing Nb composition.

Introduction

The crystal structures of TiO_2 (*1–3*), NbO_2 (4–6), and $Nb_xTi_{1-x}O_2$ (7–10) have been well-established through various diffraction studies. In $Nb_xTi_{1-x}O_2$, however, local structures made up of specific elements, such as Nb–O interactions, have not yet been elucidated because diffraction techniques lack element-specificity. That is, X-ray (and neutron) diffraction is sensitive to the short- and long-range coordination about a specific site averaged over the different atoms occupying it. In view of this, the use of synchrotron radiation for X-ray absorption spectroscopy (XAS) has received much attention (*11–13*). XAS is sensitive to the short-range coordination and valence of a specific element averaged over its different sites. Through analyses of X-ray absorption near edge structure (XANES) and extended X-ray absorption fine structure (EXAFS), the average oxidation state and coordination environment of a specific element can be determined regardless of sample crystallinity.

There are many recent reports of XAS studies of various titanium and niobium oxides: Ti K-edge XANES and EXAFS of $Nb_xTi_{1-x}O_2$ for $0.0 \leq x \leq 0.9$ by Poumellec *et al.* (*14*), and Picard-Lagnel *et al.* (*15*); Nb L-edge XANES of Nb_2O_5 by Sugiura *et al.* (*16*); Nb K-edge EXAFS and XANES of metal niobates by Nakai *et al.* (*17*); Nb K-

* To whom correspondence should be addressed.

0022-4596/91 $3.00

edge EXAFS of $Nb(OEt)_5$ by Vandenborre *et al.* (*18*); Ti K-edge EXAFS and XANES of TiO_2 by Greegor *et al.* (*19*); and Ti K-edge and Ta L-edge XANES of $Ti_{1-x}Ta_xO_2$ for $0.0 \leq x \leq 0.5$ by Poumellec *et al.* (*20*). Until now, however, no results have been reported for Nb K-edge XANES/EXAFS studies of the $Nb_xTi_{1-x}O_2$ system with the rutile structure. In the present investigation, the structure of the $Nb_xTi_{1-x}O_2$ solid solution (for $0.1 \leq x \leq 1.0$) was studied through niobium K-edge XANES and EXAFS.

Experimental Procedure

NbO_2 was prepared from Nb_2O_5 (Johnson Matthey, 99.9999% pure, metals basis) in a reducing atmosphere (5 vol% H_2 in Ar) at 1450°C for 5 hr. The heating and cooling rates were 210°/hr. Solid solutions of various x (x = 0.1, 0.2, 0.32, 0.4, 0.5, 0.6, 0.7, 0.8, and 0.9 in $Nb_xTi_{1-x}O_2$) were synthesized from mixtures of TiO_2 (Alfa Products, 99.8% pure, metals basis) and NbO_2 powders by isostatically pressing at 30,000 psi and by solid state sintering at 1400°C for 5 hr. The atmosphere for the synthesis was identical to that used for the preparation of NbO_2 powder. The synthesized solid solutions were hot-pressed in vacuum at 1250°C under 3000 psi in a graphite die. Pure TiO_2 and NbO_2 specimens were also prepared by hot pressing in the same manner. After hot pressing, the specimens were examined by X-ray diffraction (XRD) in order to ensure that the single-phase rutile structure was obtained and to determine the lattice parameters. The parameters obtained here agree with those previously published (*7, 9*).

The specimen thicknesses, t (cm), for XAS measurements in transmission mode were calculated so as to yield a unit absorption edge jump according to $t = 1/[(\mu/\rho)\rho]$, where μ/ρ (cm^2/g) is the total mass absorption coefficient at 19.05 keV and ρ (g/cm^3) is the density of the specimen. From these calculated ideal thicknesses, the specimens were prepared by mechanical grinding. The actual thicknesses were measured by using a digital micrometer with spherical tips (Mitsutoyo): some 60 measurements were made per specimen, and the average thicknesses were obtained. Unfortunately, in all but two cases, the specimens proved to be too thin and brittle to withstand grinding to the ideal thicknesses (*21*).

XAS experiments were conducted on beamline X-18B at the National Synchrotron Light Source (NSLS), Brookhaven National Laboratory. The NSLS was operated at 2.5 GeV with approximately 90–180 mA of electron current. The X-ray beam was monochromated with a channel-cut Si(220) crystal with a weak-link. In order to minimize the harmonic content of the incident X-ray beam, the monochromator was detuned to pass approximately 80% of the maximum incident photon intensity. The slit width was set to 1 mm (V) × 10 mm (H) to attain a total energy bandwidth (i.e., a Gaussian convolution of the energy divergence of the synchrotron beamline and the rocking curve width, in eV, of the Si(220) diffraction crystal) of about 5 eV at 19,000 eV. The total natural core-hole linewidth of the Nb K-edge X-ray transition is reported to be some 6 eV (*22*). Assuming that the energy bandwidth and natural linewidth add in quadrature, the overall effective spectral resolution is ca. 8 eV at 19,000 eV.

The Nb K-edge X-ray absorption data were collected under ambient conditions with a step size of 1.0 eV/pt in the XANES region (18.94 to 19.05 keV) and 0.04 $Å^{-1}$/pt in the EXAFS region (4 to 16 $Å^{-1}$). Counting times ranged from 2 to 10 sec/pt. Energy calibration was maintained to ±1.0 eV by use of a niobium foil (25 μm, A. D. MacKay): the absorption edge inflection point in the first differential XANES data for the Nb foil was set to 18,990.8 eV. The incident intensity (I_0) and the transmitted intensity (I_t) were measured using sealed-ion-chamber proportional counters with ab-

sorption lengths of 10 and 30 cm, respectively. The ion-chambers were filled with argon gas, and the pressures were adjusted to 1.19 atm for I_0 and to 1.98 atm for I_t. This gave approximately 20% absorption of I_0 and 100% absorption of I_t at 19.074 keV.

The X-ray absorption data were normalized according to a procedure similar to that described elsewhere (*23*). The preedge data were modeled with a two-term linear function, which was fitted below the onset of the absorption edge and extrapolated above the edge. The postedge data were modeled with a three-term quadratic function, which was fitted above the edge and extrapolated below the edge. The normalized data were obtained by subtracting the preedge absorption approximation from the raw data and then dividing the difference by the postedge absorption approximation. This normalization procedure facilitates a direct quantitative comparison of the shapes and intensities of features found in XANES. Further, this procedure provides normalized EXAFS data with an absorption edge jump equal to unity.

The first and the second differential XANES were obtained by use of a Fourier transformation technique (*24*). The EXAFS data reduction and analysis were performed as described elsewhere (*25*). The normalized data ($\ln(I_0/I_t)$ vs E) were converted into k-space by using an experimental threshold energy (E_0) of 19,000 eV in $k = [0.263(E - E_0)]^{1/2}$. In order to extract the EXAFS, $\chi(k)$ vs k, the postedge background absorption was modeled with five sections (3.123 $Å^{-1}$ per section) of cubic spline functions. The EXAFS, $\chi(k)$, were weighted by k^3 and Fourier transformed without phase shift correction. By applying Hanning window functions to the Fourier transform data, the oxygen coordination spheres about niobium were isolated from r-space (0.91–2.19 Å) and back-transformed to k-space. Fourier-filtered data ($k^3\chi(k)$ vs k, for $4 \leq k \leq 14$ $Å^{-1}$) were employed in the nonlinear least squares curve fitting with the single scattering theory of EXAFS (*25*). Theoretical backscatterer amplitude and phase functions for oxygen as well as a theoretical absorber phase function for niobium were used in the curve fitting (*26*). The function for niobium ($Z = 41$) was approximated by an arithmetic average of those for Zr ($Z = 40$) and Mo ($Z = 42$). Four parameters were refined in the curve fitting according to the method described by Teo *et al.* (*27*): (i) a scale factor, B; (ii) a Debye–Waller factor, σ; (iii) an interatomic distance, r; and, (iv) an energy shift ΔE_0, which is equal to $E_0^{th} - E_0$ (E_0^{th} is the theoretical threshold energy for the total phase function). Correlations within the set of parameters (ΔE_0 vs r) were examined and the corresponding phase correlation curves were employed to adjust the best fit interatomic distances, r_{Nb-O}. NbO_2 was used as the model compound because its crystallographic parameters are well-documented (*4–6*) and the oxidation state of niobium in the bulk is known, i.e., Nb^{4+}. The estimated standard deviation for the Nb–O interatomic distances is ±0.01 Å.

Results and Discussion

XANES data. Figures 1a, 1b and 1c show the normalized Nb K-edge XANES as well as the first and the second differential XANES, respectively, for the $Nb_xTi_{1-x}O_2$ solid solution for $0.1 \leq x \leq 1.0$. These XANES data are characterized by three features: (i) a weak preedge absorption shoulder at approximately 18,982 eV, which is due to an electronic transition from the Nb 1*s*-orbital to the 4*d*-orbital manifold; (ii) an absorption edge at approximately 18,996 eV, which is due to, in part, an electronic transition from the Nb 1*s*-orbital to the 5*p*-orbital manifold; and, (iii) two strong edge peaks at approximately 19,005 and 19,015 eV, which are due to low-energy scattering resonances of photoelectrons by neighboring atoms (*28–30*). Even under the low-

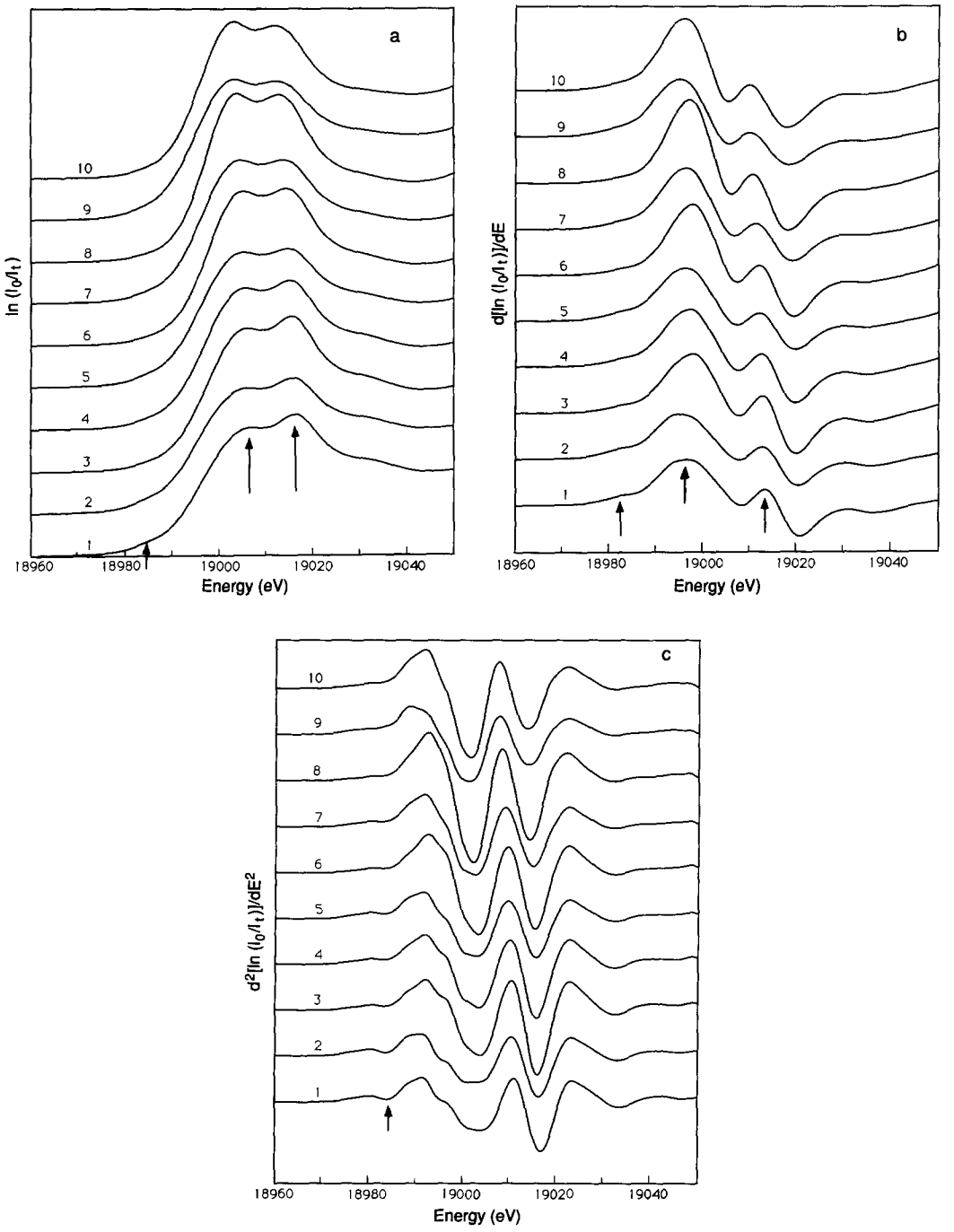

FIG. 1. (a) Normalized Nb K-edge XANES for the $Nb_xTi_{1-x}O_2$ solid solution, $0.1 \leq x \leq 1.0$. The arrows indicate the preedge shoulder and the first and second edge peaks, in order of increasing energy. (b) First differential Nb K-edge XANES. The arrows indicate the preedge and the first and second edge peak inflection points, in order of increasing energy. (c) Second differential Nb K-edge XANES. The arrow indicates the preedge peak. The preedge peak positions shown in Fig. 2 were obtained from these data. The numbers on each spectrum are: 1 for $Nb_{0.1}Ti_{0.9}O_2$; 2 for $Nb_{0.2}Ti_{0.8}O_2$; 3 for $Nb_{0.32}Ti_{0.68}O_2$; 4 for $Nb_{0.4}Ti_{0.6}O_2$; 5 for $Nb_{0.5}Ti_{0.5}O_2$; 6 for $Nb_{0.6}Ti_{0.4}O_2$; 7 for $Nb_{0.7}Ti_{0.3}O_2$; 8 for $Nb_{0.8}Ti_{0.2}O_2$; 9 for $Nb_{0.9}Ti_{0.1}O_2$; and 10 for NbO_2. The vertical scales are offset for clarity.

resolution conditions that obtain at the Nb K-edge, the XANES of Fig. 1 are clearly sensitive to electronic and geometric perturbations of niobium in $Nb_xTi_{1-x}O_2$ for $0.1 \leq x \leq 1.0$.

Inspection of the XANES, Fig. 1a, reveals an alteration in the relative intensities of the edge peaks on going from one end member to the other. For NbO_2, the normalized intensity of the peak at ca. 19,003 eV is larger than that for the peak at ca. 19,013 eV (Fig. 1a, top curve), whereas the reverse is true for $Nb_{0.1}Ti_{0.9}O_2$ (Fig. 1a, bottom curve). The first differential XANES, Fig. 1b, show a significant broadening of the main inflection point peak at ca. 18,996 eV with decreasing x. There is only minor variability in the peak shape of the secondary inflection point at ca. 19,010 eV over the entire compositional range, $0.1 \leq x \leq 1.0$. Most important, close inspection of the data in Fig. 1 reveals that the relative intensity of the preedge shoulder decreases with increasing x. This is consistent with a decrease in the average formal valence of Nb on going from $Nb_{0.1}Ti_{0.9}O_2$, with both Nb^{5+} and Nb^{4+} sites, to NbO_2, with only Nb^{4+} sites. That is, the decrease in the preedge peak intensity evident in the second differential XANES of Fig. 1c directly reflects a decrease in the density of empty d-states in order from $x = 0.1$ ($4d^{1-\delta}$ for $0 < \delta < 1$) to $x = 1.0$ ($4d^1$). Alternatively, this trend may reflect a modification of the geometry about niobium, such as a decrease in the Nb site distortion and/or a variation of the Nb–O distance, etc., with increasing x. Further evidence to support the former interpretation is provided by the variation of the position of the preedge shoulder with respect to Nb concentration, Fig. 2. The position of the preedge shoulder increases with decreasing Nb concentration. This variation of the position of the preedge shoulder is interpreted as follows: when an Nb^{4+} ion loses its outer $4d^1$ electron, the attractive potential of the nucleus on the 1s-electron increases, and

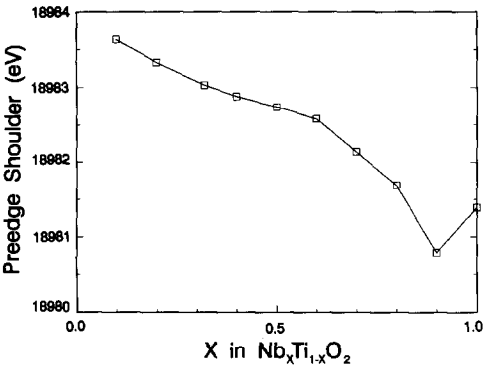

FIG. 2. Variation of the position of the preedge shoulder with respect to Nb concentration, x, in $Nb_xTi_{1-x}O_2$.

the repulsive Coulomb interaction between the core and all other electrons decreases. Therefore, the positive shift of preedge position with decreasing Nb concentration observed herein suggests that the ratio of Nb^{5+} to Nb^{4+} increases with decreasing Nb concentration. This interpretation is in accord with previous molybdenum and vanadium K-edge XANES studies, which revealed a direct correlation between the edge inflection point energy and the valence of Mo and V over a wide range of formal oxidation states (*31*). In general, an increase of 1–2 eV in preedge position is expected for an increase of valence by 1. Finally, Eror (*32*) indicates that the maximum solubility of Nb^{5+} in TiO_2 is between 4 and 8 a/o (cation atomic percent) at 1060°C in pure oxygen at 1 atm. Within this solubility limit, donor dopants (i.e., Nb) are electronically compensated by additional oxygen uptake in the oxidized state. According to Valigi *et al.* (*33*), the maximum solubility of Nb^{5+} in TiO_2 is approximately 6 a/o in a reducing atmosphere, and the extra positive charge due to Nb^{5+} is compensated by the creation of an equivalent amount of Ti^{3+}.

Based upon the analysis of Ti K-edge XANES data for the $Nb_xTi_{1-x}O_2$ solid solution ($0.0 \leq x \leq 0.9$), Poumellec *et al.* (*14*)

suggested an electron exchange between Ti^{4+} and Nb^{4+} ions because of the proximity of the two energy levels, $3d^0$ and $4d^1$, respectively. Recently, Valigi *et al.* (*33*) reported results of TGA, EPR, diffuse reflectance, and magnetic susceptibility measurements for $Nb_xTi_{1-x}O_2$, $0 \leq x \leq 0.1$. They pointed out that, if all the Nb^{4+} ions are ionized to Nb^{5+}, an equivalent amount of Ti^{3+} needs to be created to satisfy the electroneutrality condition. If this is correct, then the carrier concentration in the *d*-band, and hence the electrical conductivity, is expected to increase (unless the electrons are localized) with increasing Nb concentration. However, according to Sakata *et al.* (*34*), the dc electrical conductivity increases from TiO_2 to near $x = 0.1$, and then it decreases with further increases in Nb concentration. Thus, it appears that the results of Poumellec *et al.* (*14*) are in agreement with those of Sakata *et al.* (*34*) for $x < 0.1$. For $x > 0.1$, the results reported herein are also consistent with those of Sakata *et al.* (*34*). These can be summarized as follows: (i) At low Nb concentration, the Nb^{4+} ions are dispersed randomly in the TiO_2 matrix, and an electron transfer from Nb^{4+} to Ti^{4+} ions takes place, thereby creating Nb^{5+} ions as shown herein by XANES (vide supra) and as suggested by Poumellec *et al.* (*14*). (ii) As the Nb concentration increases, Nb ions begin to interact with each other and form Nb . . . Nb pairs, as postulated by Sakata (*7, 8, 10*). That is, the pair formation process occurs such that the Nb $4d^1$-electrons, which have been free in the Ti $3d$-band, are reclaimed by niobium and become localized as Nb^{4+} ions.

EXAFS data. The background-subtracted Nb K-edge EXAFS ($k^3\chi(k)$ vs k) and the corresponding Fourier transform data for $0.1 \leq x \leq 1.0$ in $Nb_xTi_{1-x}O_2$ are presented in Figs. 3 and 4, respectively. In the Fourier transform data for NbO_2 (Fig. 4, top curve), the principal peak at 1.46 Å (before phase shift correction) is due to backscattering

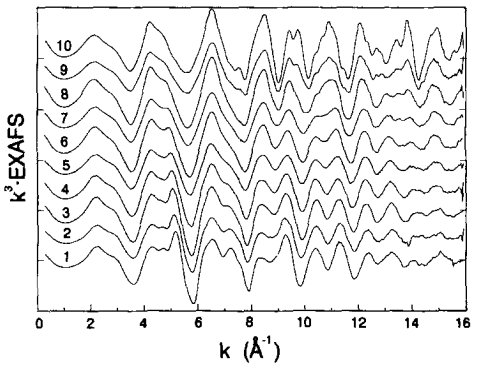

FIG. 3. Background-subtracted, k^3-weighted Nb K-edge EXAFS for the $Nb_xTi_{1-x}O_2$ solid solution, $0.1 \leq x \leq 1.0$. The numbers on each spectrum correspond to the individual phases identified in the legend to Fig. 1. Vertical scale is offset for clarity.

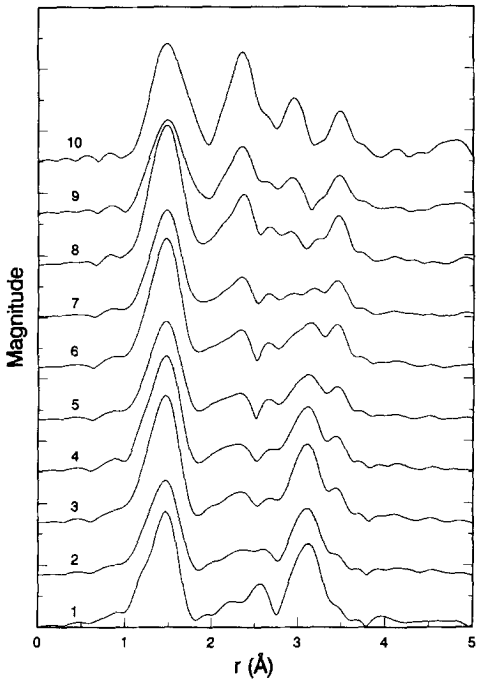

FIG. 4. Fourier transforms of the Nb K-edge EXAFS for the $Nb_xTi_{1-x}O_2$ solid solution, $0.1 \leq x < 1.0$. The numbers on each data set correspond to the individual phases identified in the legend to Fig. 1. Vertical scale is offset for clarity.

from the six nearest oxygen neighbors at an average distance of 2.06 Å about Nb (*6*). NbO_2 has a rutile-type structure with a range of Nb–O bond lengths of 1.92–2.23 Å (*6*) and a static displacement about the average Nb–O distance (2.06 Å) of 0.085 Å (*35*). The three distant peaks between 2 and 4 Å in the Fourier transform data for NbO_2 are due to backscattering from niobium neighbors at 2.743, 3.256, and approximately 3.7 Å about Nb (*6*). Figure 4 indicates that the intensities of the three Nb . . . Nb peaks gradually decrease with decreasing Nb concentration. Also, as the Nb concentration decreases, two new peaks at approximately 2.6 and 3.1 Å (before phase shift correction) due to backscattering from titanium start to evolve. In fact, the Fourier transform of the Nb K-edge EXAFS for $Nb_{0.1}Ti_{0.9}O_2$ (Fig. 4, bottom curve) is nearly identical to that of the Ti K-edge EXAFS for TiO_2, rutile (*15, 36*). The overall intensities of the Nb . . . Nb/Ti peaks in the Fourier transform data for $Nb_xTi_{1-x}O_2$ decrease gradually from $x = 1.0$ to 0.7 and, then, increase from $x = 0.6$ to 0.1. This diminution of the Nb . . . Nb/Ti peaks is due to, in part, a phase difference of approximately π radians between Nb . . . Nb and Nb . . . Ti backscatterings. The destructive interference of backscatterer phase shifts for Ti and Nb is predicted for $k \geq 7$ Å^{-1} from the theoretical functions (*26*). Similar phase cancellation effects were previously noted for Ti . . . Ti and Ti . . . Nb backscattering (*15*), Fe . . . Fe and Fe . . . Mo backscattering (*37*), Ni . . . Mg and Ni . . . Ni backscattering (*38, 39*), *M* . . . Ni and *M* . . . Mo backscattering (*M* ≡ Mo, Ni) (*40*), and Ti . . . Zn and Ti . . . Si backscattering (*41*). The combination of the phase cancellation effects and, in the case of a random distribution of Nb and Ti cations in $Nb_xTi_{1-x}O_2$, the complexities of appropriate numerical models prevented a detailed curve fitting analysis of the Nb . . . Nb/Ti interactions with the available EXAFS.

The average niobium–oxygen interatomic distances (r_{Nb-O}) as a function of x in $Nb_xTi_{1-x}O_2$ are presented in Fig. 5. In the same figure, the average metal–oxygen (*M*–O, *M* ≡ Nb and Ti) distances (r_{M-O}) calculated from the neutron diffraction data reported by Yamada *et al.* (*9*) are plotted for comparison. The r_{M-O} values were calculated from $r_{M-O} = [2r_{M-O,(110)} + 4r_{M-O,Other}]/6$. Here, $r_{M-O,(110)}$ is the *M*–O distance on the (110) plane (i.e., the *M*–O distance from the body-centered metal to the oxygen at the vertex of the octahedra) and $r_{M-O,Other}$ is that on the plane perpendicular to (110) (i.e., the *M*–O distance on the base of the octahedra). In Fig. 5, it is noticed that r_{Nb-O} increases linearly with increasing Nb concentration, and that r_{Nb-O} is larger than r_{M-O}. Since the radius of the Nb^{4+} ion is larger than that of the Ti^{4+} ion (*42*), r_{Nb-O} is expected to be larger than r_{M-O}.

The clear decrease of the Nb–O distance with decreasing Nb concentrations in the $Nb_xTi_{1-x}O_2$ series (Fig. 5) suggests an increase in the number of Nb cations with

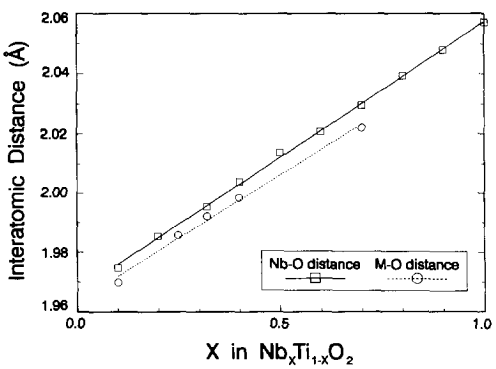

FIG. 5. Variation of the average Nb–O interatomic distance (r_{Nb-O}) with respect to Nb concentration, x, in $Nb_xTi_{1-x}O_2$. For comparison, the variation of the average metal–oxygen interatomic distance (r_{M-O}, *M* ≡ Nb and Ti) calculated from the neutron diffraction data of Yamada *et al.* (*9*) is also shown. The solid and dashed lines for r_{Nb-O} and r_{M-O}, respectively, were obtained from least squares fits.

oxygen coordination lower than that for pristine NbO_2 (*6*) as a function of decreasing x. In particular, the results are consistent with an increasing occupation of tetrahedral interstitial sites, with short Nb–O distances, as a function of decreasing x. The principal fraction of Nb ions would, as expected, occupy the regular octahedral cation sites, with long Nb–O distances. This interpretation is in line with the neutron diffraction study of Yamada *et al.* (*9*), which showed that at low Nb concentrations, Nb ions enter into TiO_2 by occupying tetrahedral (T_d) interstitial sites as well as regular cation octahedral (O_h) sites. For $Nb_{0.1}Ti_{0.9}O_2$, approximately 20% of the total Nb ions occupy tetrahedral interstitial sites and the remaining 80% occupy octahedral sites (i.e., $Nb^{T_d}_{0.02}Nb^{O_h}_{0.08}Ti_{0.9}O_2$). For such a distribution of Nb cations among tetrahedral and octahedral sites, the average oxygen coordination number is 5.6, i.e., $[0.2 \times 4] + [0.8 \times 6]$. In the analysis of EXAFS, it is generally recognized that accurate coordination numbers are significantly more troublesome to determine than are interatomic distances. Even with high-quality data, it is very difficult to obtain coordination numbers with an uncertainty of less than $\pm 10\%$, e.g., $6 \pm \frac{1}{2}$ atoms.

In this investigation, the preparation of thin specimens (20–100 μm) of the calculated ideal thicknesses was not possible to achieve; thus, it was impossible to avoid so-called thickness effects (*43*). It is well-known that the thickness effect has a large detrimental influence on EXAFS-determined coordination numbers (*44–48*). Therefore, with the available data, it was not possible to obtain oxygen coordination numbers of sufficient accuracy to distinguish between a coordination number of 6 for NbO_2, on the one hand, and 5.6 for $Nb_{0.1}Ti_{0.9}O_2$, on the other. Although several reports have dealt with the thickness effect by using various after-the-fact numerical treatments (*44–48*), none of these corrections was found to compensate the thickness artifacts observed in the present work. For future Nb X-ray absorption measurements of the $Nb_xTi_{1-x}O_2$ system, the use of electron-yield signal detection, which is not susceptible to thickness artifacts (*49, 50*), is recommended.

Conclusions

The initial results of niobium K-edge X-ray absorption studies of the $Nb_xTi_{1-x}O_2$ solid solution ($0.1 \leq x \leq 1.0$) with the rutile structure have been described. For 10 compositions of this NbO_2–TiO_2 system (i.e., x = 0.1, 0.2, 0.32, 0.4, 0.5, 0.6, 0.7, 0.8, 0.9, and 1.0), the element specificity of the XANES and EXAFS techniques was exploited to probe the site symmetry and valence of niobium. Even at ca. 19,000 eV where low-resolution conditions prevail (due to the combined effects of the monochromator bandwidth and the natural core-hole linewidth), the Nb K-edge XANES was shown to be a sensitive indicator of the valence of niobium. Analysis of the XANES revealed that the formal valence of a small fraction of niobium cations increases from 4+ to 5+ with decreasing Nb concentration, x. This suggests that the $4d^1$ electrons of Nb^{4+} are either donated to or shared with Ti^{4+} ions ($3d^0$) at low Nb concentrations. The collection and analysis of high-resolution Nb L_1-, L_2- and L_3-edge XANES (ca. 2370 to 2700 eV) for the $Nb_xTi_{1-x}O_2$ solid solution is expected to provide further detailed insights about the electronic and geometric properties of niobium. The results of the Nb K-edge EXAFS analysis clearly indicate a contraction of the Nb–O interatomic distance with decreasing Nb concentration. These results are consistent with an increasing occupation of tetrahedral interstitial sites, with short Nb–O distances, as a function of decreasing x in $Nb_xTi_{1-x}O_2$. The principal fraction of the niobium ions

occupies regular octahedral cation sites, with long Nb–O distances, at low x.

Acknowledgments

We thank Drs. Arun Bommannavar and Mohan Ramanathan for their assistance with the X-ray absorption measurements at the NSLS, which is supported by the U.S. Department of Energy, Division of Materials Sciences and Division of Chemical Sciences. One of the authors (I.S.) acknowledges the receipt of a scholarship from the Carborundum Co. (Niagara Falls, New York) during the course of this investigation.

References

1. S. C. Abrahams and J. L. Bernstein, *J. Chem. Phys.* **55,** 3206 (1971).
2. T. M. Sabine and C. J. Howard, *Acta Crystallogr. Sect. B* **38,** 701 (1982).
3. J. K. Burdett, T. Hughbanks, G. J. Miller, J. W. Richardson, Jr., and J. V. Smith, *J. Am. Chem. Soc.* **109,** 3639 (1987).
4. T. Sakata, K. Sakata, and I. Nishida, *Phys. Status Solidi* **20,** K155 (1967).
5. R. Pynn, J. D. Axe, and R. Thomas, *Phys. Rev. B* **13,** 2965 (1976).
6. A. K. Cheetham and C. N. R. Rao, *Acta Crystallogr. Sect. B* **32,** 1579 (1976).
7. K. Sakata, *J. Phys. Soc. Jpn.* **26,** 1067 (1969).
8. K. Sakata, *Acta Crystallogr. Sect. B* **35,** 2836 (1979).
9. H. Yamada, R. G. Teller, and I. Song, *in* "Proceedings of the 1989 Materials Research Society Symposium" Vol. 138, pp. 185–190 (1989).
10. K. Sakata, *J. Phys. Soc. Jpn.* **26,** 582 (1969).
11. P. Lagarde, D. Raoux and J. Petiau, (Eds.), *EXAFS and Near-Edge Structure IV, J. Phys. Collogue C8, Suppl. 12,* **47,** C8-1–C8-1243 (1986).
12. D. C. Koningsberger and R. Prins, (Eds.), *X-ray Absorption. Principles, Applications, Techniques of EXAFS, SEXAFS, and XANES,* pp. 1–673, Wiley, New York (1988).
13. J. M. deLeon, E. A. Stern, D. E. Sayers, Y. Ma, and J. J. Rehr (Eds.), *XAFS V, Proceedings of the Fifth International Conference on X-ray Absorption Fine Structure, Physica B* **158,** 1–732 (1989).
14. B. Poumellec, F. Lagnel, J. F. Marucco, and B. Touzelin, *Phys. Status Solidi B* **133,** 371 (1986).
15. F. Picard-Lagnel, B. Poumellec, and R. Cortes, *J. Phys. Chem. Solids* **50,** 1211 (1989).
16. C. Sugiura, M. Kitamura, and S. Muramatsu, *J. Phys. Chem. Solids* **49,** 1095 (1988).
17. I. Nakai, J. Akimoto, M. Imafuku, R. Miyawaki, Y. Sugitani, and K. Koto, *Phys. Chem. Miner.* **15,** 113 (1987).
18. M. T. Vandeborre, B. Poumellec, C. Alquier, and J. Livage, *J. Non-Cryst. Solids* **108,** 333 (1989).
19. R. B. Greegor, F. W. Lytle, D. R. Sandstrom, J. Wong, and P. Schultz, *J. Non-Cryst. Solids* **55,** 27 (1983).
20. B. Poumellec, J. F. Marucco, and B. Touzelin, *Phys. Status Solidi B* **137,** 519 (1986).
21. I. Song, Ph.D. dissertation, Case Western Reserve University, Cleveland, OH, (1990).
22. O. Keski-Rahkonen and M. O. Krause, *At. Nucl. Data Tables* **14,** 139 (1974).
23. M. R. Antonio, R. G. Teller, D. R. Sandstrom, M. Mehicic, and J. F. Brazdil, *J. Phys. Chem.* **92,** 2939 (1988).
24. D. G. Cameron and D. J. Moffatt, *J. Test. Eval.* **12,** 78 (1984).
25. B. K. Teo, "EXAFS: Basic Principles and Data Analysis," pp. 79–157, Springer-Verlag, Berlin, (1986).
26. B. K. Teo and P. A. Lee, *J. Am. Chem. Soc.* **101,** 2815 (1979).
27. B. K. Teo, M. R. Antonio, and B. A. Averill, *J. Am. Chem. Soc.* **105,** 3751 (1983).
28. F. Sette, J. Stohr, and A. P. Hitchcock, *Chem. Phys. Lett.* **110,** 517 (1984).
29. A. Bianconi, E. Fritsch, G. Calas, and J. Petiau, *Phys. Rev. B* **32,** 4292 (1985).
30. F. W. Lytle, R. B. Greegor, and A. J. Panson, *Phys. Rev. B* **37,** 1550 (1988).
31. S. P. Cramer, T. K. Eccles, F. W. Kutzler, K. O. Hodgson, and L. E. Mortenson, *J. Amer. Chem. Soc.* **98,** 1287 (1976); J. Wong, F. W. Lytle, R. P. Messmer, and D. H. Maylotte, *Phys. Rev. B* **30,** 5596 (1984).
32. N. G. Eror, *J. Solid State Chem.* **38,** 281 (1981).
33. M. Valigi, D. Cordischi, G. Minelli, P. Natale, and C. P. Keijzers, *J. Solid State Chem.* **77,** 255 (1988).
34. K. Sakata, I. Nishida, M. Matsushima, and T. Sakata, *J. Phys. Soc. Jpn.* **27,** 506 (1969).
35. The static displacement, σ, was calculated according to the equation $\sigma = \Sigma_i[(r_i - \bar{r})^2/N]^{1/2}$, where $\bar{r}$ is the average Nb–O distance, r_i are the individual Nb–O distances, and N is the number (12) of individual Nb–O distances, as described in M. R. Antonio, B. K. Teo, and B. A. Averill, *J. Am. Chem. Soc.* **107,** 3583 (1985).
36. H. Morikawa, T. Osuaka, F. Maurmo, A. Yasumori, and M. Momura, *J. Non-Cryst. Solids* **82,** 97 (1986).
37. M. R. Antonio, B. K. Teo, W. E. Cleland, and B. A. Averill, *J. Am. Chem. Soc.* **105,** 3477 (1983).

38. A. MANCEAU AND G. CALAS, *Am. Mineral.* **70,** 549 (1985).
39. A. MANCEAU AND G. CALAS, *Clay Miner.* **21,** 341 (1986).
40. B. K. TEO, H. S. CHEN, R. WANG, AND M. R. ANTONIO, *J. Non-Cryst. Solids* **58,** 249 (1983).
41. T. DUMAS AND J. PETIAU, *J. Non-Cryst. Solids* **81,** 201 (1986).
42. R. D. SHANNON AND C. T. PREWITT, *Acta Crystallogr. Sect. B* **25,** 925 (1969).
43. L. G. PARRATT, C. F. HEMPSTEAD, AND E. L. JOSSEM, *Phys. Rev.* **105,** 1228 (1957).
44. E. A. STERN AND K. KIM, *Phys. Rev. B* **23,** 3781 (1981).
45. Z. TAN, J. I. BUDNICK, AND S. M. HEALD, *Rev. Sci. Instrum.* **60,** 1021 (1989).
46. S. M. HEALD, *in* "X-ray Absorption: Principles, Applications, Techniques of EXAFS, SEXAFS, and XANES" (D. C. Koningsberger and R. Prins, Eds.), pp. 87–118, Wiley, New York (1988).
47. J. GOULON, C. GOULON-GINET, R. CORTES, AND J. M. DUBOIS, *J. Phys.* **43,** 539 (1982).
48. J. GOULON, C. GOULON-GINET, R. CORTES, AND J. M. DUBOIS, *in* "EXAFS and Near Edge Structure, Proceedings of the 1982 International Conference" (A. Bianconi, L. Incoccia, and S. Stipcich, Eds.), pp. 96–97, Springer-Verlag, New York (1983).
49. W. T. ELAM, J. P. KIRKLAND, R. A. NEISER, AND P. D. WOLF, *Phys. Rev. B* **38,** 26 (1988).
50. A. ERBIL, G. S. CARGILL, R. FRAHM, AND R. F. BOEHME, *Phys. Rev. B* **37,** 2450 (1988).